Modeling and Robust Body Freedom Flutter Analysis of Flexible Aircraft Configurations

Andrea Iannelli, Andres Marcos and Mark Lowenberg[1]

***Abstract*— Body Freedom Flutter (BFF) is a dynamic instability concerning coupling between rigid-body and elastic modes of the aircraft. Flexible configurations with adverse geometric properties have been found susceptible to this phenomena. In this work a simple model, based on the typical section framework and incorporating basic features of the problem, is proposed. A sensitivity study of the role played by two meaningful parameters (wing bending stiffness and tail horizontal distance) is performed both with classical (p-k method) and robust (μ technique) tools. The analyses performed showcase the potential and prowess of the latter, not only in inferring critical features of BFF but also in its capability for more complete and complex robust parametric analysis.**

I. Introduction

The coupled problem of a flexible structure surrounded by a fluid flow generating a pressure depending on its geometry is the subject of aeroelasticity. The interaction among inertial, elastic and aerodynamic forces can lead to critical phenomena as flutter, which is a self-excited instability whose level of vibration may result in sufficiently large amplitudes to provoke failure. It is common practice to assume the occurrence of a lifting surface's flutter as unrelated to the rigid-body motion of the vehicle where it is mounted, and thus it is extensively accepted to rely on *restrained* body models (e.g. cantilever wing).

However, recent studies [1], [2] have demonstrated that structural sizing aimed to achieve very light weight structure, and thus a significant degree of flexibility, could lead to multiple flutter mechanisms. In particular, a detrimental coupling between the rigid-body modes and the first elastic modes of the vehicle could arise, leading to the so-called Body Freedom Flutter. Air vehicle layout in terms of geometry and stability derivatives plays also a decisive role in the extent of this phenomena. As a result, the aeroelastic sizing required to ensure flutter free behavior of the vehicle entails a multidisciplinary approach.

Furthermore, it is acknowledged that flutter analysis in general doesn't provide highly confident numerical predictions due to simplifying modeling assumptions and to their sensitiveness to small variations in parameter values [3], which are often only estimated. In addressing this issue, in the last decades researchers looked at robust modeling and analysis techniques from the robust control community, specifically Linear Fractional Transformation (LFT) models and μ analysis [4]. The so-called flutter robust analysis [5], [6] aims to quantify the gap between the prediction of the nominal stability analysis (i.e. model without uncertainties) and the worst prediction when the whole set of uncertainty is contemplated. This results in a powerful tool when used as a complement to the classic techniques in that it can highlight weak points of the model requiring more refinement and conversely identify parameters that can be coarsely estimated as they do not have a strong influence on the results.

In this work the capability of the typical section framework in studying flutter of simple wing geometries is addressed first and validated against the Goland wing, a well-known benchmark problem from this field's literature (Section II). Then an elementary model to study BFF is proposed, that includes: longitudinal dynamic of the vehicle described by its angle of attack and pitch rate (the so-called *short period approximation*), the first bending and torsional modes, and their coupling terms (Section III). A range of aircraft configurations, differing in geometric properties and degree of flexibility, are analyzed within this framework and the results, in terms of mismatch between restrained and BFF model predictions, are discussed (Section IV). Introduced by a cursory description of LFT and μ analysis, finally the robust BFF analysis (Section V) is performed in order to show how μ analysis can be advantageously employed to highlight critical parameters of the problem and quantitatively assess stability degradation due to uncertainties in the models.

II. Restrained Flutter Analysis

A. Typical section model

The *typical section* model was introduced in the early stages of aeroelasticity to investigate dynamic phenomena such as flutter [7]. Despite its simplicity, it captures essential effects in a simple model representation, see Fig. 1.

From the structural side, it basically consists of a rigid airfoil with lumped springs simulating the degrees of freedom of the section, in this case limited to plunge h and pitch α (optionally also the trailing edge flap could be considered). The main parameters in the model, refer to Fig.1, are: K_h and K_α respectively the bending and torsional stiffness; half chord b; dimensionless distances a from mid-chord to flexural axis and x_α from flexural axis to airfoil center of gravity. The position of the relevant points elastic axis (EA), center of gravity (CG) and the aerodynamic center (AC) is also marked.

For the aerodynamic loads model, the unsteady formulation proposed by Theodorsen [7] is employed. This approach is

*This work has received funding from the European Union's Horizon 2020 research and innovation programme under grant agreement No 636307, project FLEXOP.

[1] Andrea Iannelli, Andres Marcos and Mark Lowenberg are with the Department of Aerospace Engineering, University of Bristol, BS8 1TR, United Kingdom andrea.iannelli/andres.marcos/m.lowenberg@bristol.ac.uk

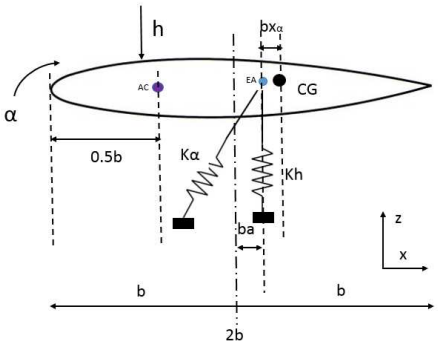

Fig. 1. Typical section sketch

based on the assumption of a thin airfoil moving with small harmonic oscillations in a potential and incompressible flow.

The premise of the typical section modeling is that the dynamics of an actual wing can be simulated choosing the aforementioned properties to match those at a span station about 70% distant from the centerline. Experience has confirmed that this assumption is reasonable for wings configurations having large aspect ratio, small sweep angle and spanwise characteristics varying smoothly.

In order to present the basic model development approach, $\mathbf{X}^E(t)$ and $\mathbf{L_a}^E(t)$ are respectively defined as the vectors of the elastic degrees of freedom and the corresponding aerodynamic loads:

$$\mathbf{X}^E(t) = \begin{bmatrix} \frac{h(t)}{b} \\ \alpha(t) \end{bmatrix}; \quad \mathbf{L_a}^E(t) = \begin{bmatrix} -L(t) \\ M^A(t) \end{bmatrix} \tag{1}$$

The set of differential equations describing the dynamic equilibrium can then be recast in matrix form using Lagrange's equations:

$$\big[\mathbf{M_s}\big]\ddot{\mathbf{X}}^E + \big[\mathbf{K_s}\big]\mathbf{X}^E = \mathbf{L_a}^E \tag{2}$$

where $\big[\mathbf{M_s}\big]$ and $\big[\mathbf{K_s}\big]$ are respectively the structural mass and stiffness matrices (structural damping is assumed null). They can be written as:

$$\big[\mathbf{M_s}\big] = m_w b \begin{bmatrix} 1 & x_\alpha \\ x_\alpha & r_\alpha^2 \end{bmatrix}; \quad \big[\mathbf{K_s}\big] = \begin{bmatrix} bK_h & 0 \\ 0 & \frac{K_\alpha}{b} \end{bmatrix} \tag{3}$$

where m_w is the mass ratio (wing weight per unit span) and r_α is the dimensionless radius of gyration of the section about the elastic axis.

Theodorsen model provides an expression of $\mathbf{L_a}^E$ in the Laplace s domain framework as:

$$\mathbf{L_a}^E(s) = q\big[\mathbf{A}(\bar{s})\big]\mathbf{X}^E(s) \tag{4}$$

where the dynamic pressure q and the dimensionless Laplace variable $\bar{s}$ (=$s\frac{b}{V}$ with V the wind speed) are introduced. $\big[\mathbf{A}(\bar{s})\big]$ is called the generalized (complex-valued) Aerodynamic Influence Coefficient (AIC) matrix. The final aeroelastic equilibrium is written in frequency-domain as:

$$\Big[\big[\mathbf{M_s}\big]s^2 + \big[\mathbf{K_s}\big] - q\big[\mathbf{A}(\bar{s})\big]\Big]\mathbf{X}^E(s) = \mathbf{0} \tag{5}$$

B. Application to wing flutter analysis

The first goal of this work is to show how this formulation can be used to evaluate the flutter speed of a finite span (3D) wing. As benchmark for this assessment the Goland wing [8] is selected. It consists of a uniform rectangular wing with constant structural and inertial properties along the span. Wing elasticity is described by means of the bending stiffness EI and torsional stiffness GJ.

An equivalence in terms of the first *uncoupled* bending and torsional natural frequencies [9] of a cantilever beam is imposed in order to find the values for the typical section stiffness parameters K_h and K_α.

$$\begin{aligned} \omega_b &= \Big(0.597\frac{2\pi}{L}\Big)^2\sqrt{\frac{EI}{m_s}} = \sqrt{\frac{K_h}{m_s}} \\ \omega_t &= \frac{\pi}{L}\sqrt{\frac{GJ}{I_\alpha}} = \sqrt{\frac{K_\alpha}{I_\alpha}} \end{aligned} \tag{6}$$

Flutter analysis studies the conditions at which the dynamic aeroelastic system loses its stability, as the air stream speed V is increased. The result is the prediction of the so-called flutter speed V_f, below which the system is guaranteed to be stable. The major methods used to accomplish this task are based on frequency-domain as this is the framework where the aerodynamics loads are most often expressed. The p-k method is employed next to analyse the wing's nominal flutter. The objective is to find the flutter determinant roots s such that nonzero solutions for $\mathbf{X}^E$ exist in (5). The complexity arises since the AIC matrix does not have a polynomial dependence on s and thus iterative solutions have to be sought.

In Fig. 2 the eigenvalues corresponding to the two modes are depicted as the airstream speed is increased. The system exhibits an instability dominated by the torsion mode, with a flutter speed V_f=141 $\frac{m}{s}$. This shows a satisfactory matching (error below 3%) with results in [8] which comprise 3D effects.

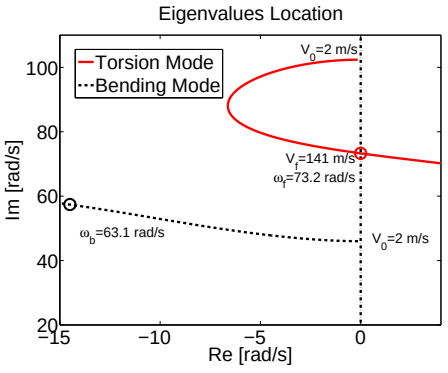

Fig. 2. Goland wing: eigenvalues location as a function of speed and frequency's value at flutter speed

III. Body Freedom Flutter Modeling

In aircraft design, vehicle dynamics modeling and analysis are often addressed considering separately the rigid-body dynamics and the structural dynamics, on account of a wide frequency separation between the two natural modes set. However, the increasing effort towards an optimal structural

sizing and lightweight material selection on one side, and the conception of geometric layout with low static stability (or rather statically unstable) compensated with full-authority control systems on the other, are reducing the applicability of the aforementioned hypothesis, enhancing the coupling between the rigid and flexible dynamics.

Reference [10], which provides a comprehensive study on the different aspects of this broad subject, is here adopted for the development of a simple framework to deal with this phenomena. The noninertial vehicle-fixed coordinate frame used to derive the equations of motion is the so-called *mean axes*. It has the properties that the origin is coincident with the instantaneous center of mass of the vehicle and the relative translational and angular momenta (about the origin) due to elastic deformation of the structure undergoing unforced vibrations are null. This choice is instrumental to avoid *inertial* coupling between the rigid-body and elastic degrees of freedom.

Only the longitudinal dynamic is retained in this model, which is described by: the vehicle angle of attack $\bar{\alpha}$, the pitch angle $\bar{\theta}$ and its pitch rate $\bar{q}$. This is the *short period approximation*, which for conventional aircraft involves rapid heave and pitch oscillations at almost constant translational speed. As testified in [2], the phugoid mode has a marginal role in BFF and thus surge velocity is neglected. Therefore, the rigid-body motion equilibrium can be written in frequency domain (for level flight) as

$$\begin{aligned} &\begin{bmatrix} (V - Z_{\dot{\bar{\alpha}}})s - Z_{\bar{\alpha}} & -(Z_{\bar{q}} + V)s \\ -(M_{\dot{\bar{\alpha}}}s + M_{\bar{\alpha}}) & s^2 - M_{\bar{q}}s \end{bmatrix} \begin{bmatrix} \bar{\alpha}(s) \\ \bar{\theta}(s) \end{bmatrix} = \begin{bmatrix} 0 \\ 0 \end{bmatrix} \\ &\mathbf{X}^R(s) = \begin{bmatrix} \bar{\alpha}(s) \\ \bar{\theta}(s) \end{bmatrix}; \;\; \bar{q} = s\bar{\theta} \end{aligned} \tag{7}$$

Where the vector of rigid degrees of freedom $\mathbf{X}^R$ and the aircraft stability derivatives $Z_{\bar{\alpha}}$, $Z_{\dot{\bar{\alpha}}}$, $Z_{\bar{q}}$, $M_{\bar{\alpha}}$, $M_{\dot{\bar{\alpha}}}$, $M_{\bar{q}}$ have been introduced. They are evaluated with first approximation formula [10].

The final task is to determine the coupling terms, since the equilibrium of the elastic degrees of freedom has already been stated in (5). The crucial aspects to address are the understanding of how the deformation affects the overall aerodynamic forces generated by the vehicle, and how the motion of the vehicle contributes to change the loads acting on the structure. A proposed simplification commonly accepted [11] is to consider fuselage and tail as rigid, which means that all the elasticity is concentrated in the wing.

The effect of the elastic deformation on the lift generated by the local wing sections is highlighted by the expression of the local angle of attack α_{loc}

$$\alpha_{loc} = \alpha_0 + \alpha + \frac{\dot{h}}{V} \tag{8}$$

where α_0 is the rigid angle of attack of the section, related to $\bar{\alpha}$. The aeroelastic stability derivatives describing the effect of deformation on the vehicle forces and moments can then be derived starting from the expression of the wing lift coefficient C_{LW}, comprising rigid and elastic effects:

$$\begin{aligned} C_{LW} &= C^R_{LW} + C^E_{LW} \\ C_{LW} &= C_{L_\alpha}(\alpha_0 + \alpha + \frac{\dot{h}}{V}) \\ C^R_{LW} &= C_{L_\alpha}\alpha_0 \\ C^E_{LW} &= C_{L_\alpha}(\alpha + \frac{\dot{h}}{V}) \end{aligned} \tag{9}$$

The latter coefficient enables thus to relate the elastic deformation to the vehicle loads. Note that for these coupling terms, determining the effect from Elastic to Rigid, the hypothesis of quasi-steadiness has been assumed. The main reason is that these terms enter the equilibrium of the rigid DOFs of the plant and thus, it is desired to keep consistency with the assumptions taken in evaluating the aerodynamic stability derivatives in Eq.7.

Vehicle rigid motion governed by (7) determines in turn the loads ${\mathbf{L_a}}^R$ acting on the wing. In particular a change in angle of attack $\bar{\alpha}$ and pitch rate $\bar{q}$ causes terms of the type of $\frac{\dot{h}}{b}$ and α (from $\mathbf{X}^E$ in (1)) to originate loads on the structure, as introduced in (4). Thus it is possible to write this cross-coupling term as:

$${\mathbf{L_a}}^R(s) = q\big[\mathbf{A}(\bar{s})\big]\big[\mathbf{T}\big]\mathbf{X}^R(s) \tag{10}$$

with $\big[\mathbf{T}\big]$ a transformation matrix which allows to express the typical section degrees of freedom in terms of $\mathbf{X}^R$.

A short-hand expression of the overall equilibrium is

$$\begin{aligned} &\left[s^2 \begin{bmatrix} \boldsymbol{M_{RR}} & \boldsymbol{M_{RE}} \\ \boldsymbol{M_{ER}} & \boldsymbol{M_{EE}} \end{bmatrix} + s \begin{bmatrix} \boldsymbol{C_{RR}} & \boldsymbol{C_{RE}} \\ \boldsymbol{C_{ER}} & \boldsymbol{C_{EE}} \end{bmatrix} + \right. \\ &\left. \begin{bmatrix} \boldsymbol{K_{RR}} & \boldsymbol{K_{RE}} \\ \boldsymbol{K_{ER}}(\bar{s}) & \boldsymbol{K_{EE}}(\bar{s}) \end{bmatrix} \right] \begin{bmatrix} \mathbf{X}^R(s) \\ \mathbf{X}^E(s) \end{bmatrix} = \begin{bmatrix} \mathbf{0} \\ \mathbf{0} \end{bmatrix} \end{aligned} \tag{11}$$

with the subscripts highlighting the kind of influence terms, e.g RE is from elastic to rigid while EE is elastic on elastic.

The intrinsic simplicity of this framework has to be ascribed to the choice of the typical section as representative of the structural dynamics of the wing. However, note that the basic physical features of the rigid-elastic coupling are kept. As shown in [10], the aeroelastic derivatives calculation process is prompted by the same line of reasoning, with integrals employed to take into account variability of the properties along the span. Moreover, it is known [12] that BFF is well predicted using linear models for the aircraft and is not the result of non-linear aerodynamics or structural nonlinearities.

IV. Nominal Analysis

A. Air vehicle configuration

The aircraft geometry used in this work to perform the BFF analyses is presented in Fig. 3. It is remarked here that this study is not aimed at investigating stability of a specific existent air vehicle layout. The chief goal is instead to show that the simple model described above enables to highlight reckoned features of BFF. Although it is claimed that BFF is a phenomena concerning mostly flying wing, it is reported in

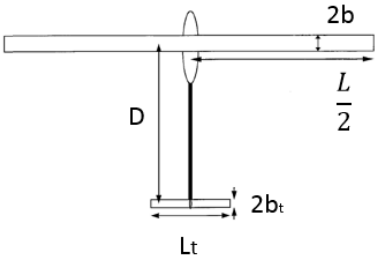

Fig. 3. Aircraft Model Geometry

literature [12] that wing/fuselage/tail configurations can also undergo this instability for an adverse combination of design parameters.

The wing is described by the parameters defining Goland wing [8], with the only exception of EI, which is assumed as a design variable that reflects the tendency towards a lightweight-oriented structural sizing. This design variable is given by EI=$\sigma_s EI_G$ with EI_G set as the Goland wing value and σ_s therefore defined as a free parameter capturing the range of bending stiffness and taking values from 0.05 (maximum bending flexibility) to 1 (maximum bending rigidity). The wing mass ratio m_w is kept constant at the Goland wing value since it is assumed to trade stiffness off for payload capability on the wing and thus no overall weight reduction is achieved. Torsional stiffness is also kept constant because as shown in Fig. 2 torsion is dominating the flutter behavior of this wing and thus a design constraint in terms of its lower value is assumed to hold.

Finally, the parameters defining the geometric and inertial properties of the aircraft are obtained scaling the values in [11] considering Goland wing mass and length as reference. The position of the tail D is considered a free parameter, as previously done for the bending stiffness. It is acknowledged indeed that the coupling of the rigid-body short period and wing first bending mode resulting in BFF is enhanced in low tail volume V_H configurations. This parameter is defined as

$$V_H = (\bar{X}_{acH} - \bar{X}_{CG})\frac{S_H}{S} \tag{12}$$

where $\bar{X}_{acH}$ and $\bar{X}_{CG}$ are respectively the dimensionless (dividing by the mean aerodynamic chord) distance of tail aerodynamic center and aircraft center of gravity from the nose, S_H and S are the tail and wing surface. Thus, once the lifting surfaces sizes are fixed, V_H is a function of D, which is expected to vary in a range between 5 m and 10 m in order to be compatible with the static stability requirement.

B. Results

Fig. 4 shows the flutter speed V_f, i.e. the lowest speed at which the system loses stability, calculated considering variations in the aforementioned design parameters (EI, D).

The first feature, familiar to aeroelasticians [7], is that the tendency for instability is more pronounced as the bending ω_b and torsional ω_t frequencies become closer. This is seen by the curve representing the restrained wing (solid line in Fig. 4), where it is evident how V_f increases as σ_s (equivalently EI) is reduced. This is due to the fact that

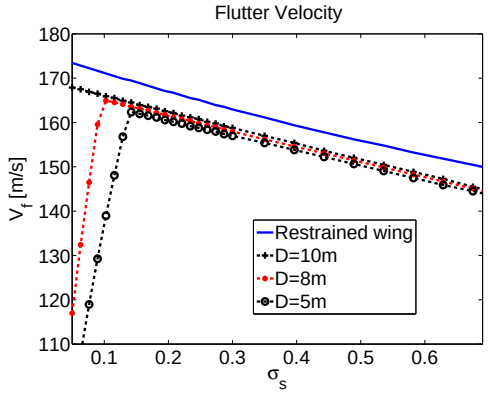

Fig. 4. Flutter speed of the simplified aircraft as the two design variables EI and D vary

a decrease in EI implies an analogous trend in the bending frequency, as expressed by (6). Since the torsional stiffness is kept constant in these analyses, a decrease in σ_s can be then interpreted as a reduction in the ratio between the uncoupled bending and torsional natural frequencies.

The flutter velocities evaluated within the BFF model (curves for D=5,8,10m) maintain this trend too, as long as the tail volume of the vehicle doesn't become critical to the stability. In fact, there is a whole range of degree of bending flexibility of the wing ($0.2<\sigma_s<1$) where V_H proves to be negligible to flutter occurrence and the BFF model predicts a relatively small decrease in flutter speed with respect to the restrained model. As the bending flexibility increases ($\sigma_s<0.2$), it becomes distinct the interaction between the short-period and the bending mode, which leads to an abrupt decrease of flutter speed. Tail volume is confirmed to play a crucial role both in prompting rigid-elastic coupling (as it changes the σ_s threshold at which the leap occurs) and in the V_f value itself. Fig. 4 clearly shows how a lower V_H (i.e. lower D) anticipates the transition to BFF mechanism and determines a lower flutter speed than for the scenario with greater V_H.

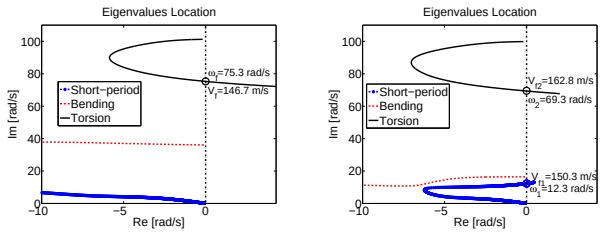

(a) σ_s=0.6 and D=5m; torsional-bending instability

(b) σ_s=0.12 and D=5m; BFF instability

Fig. 5. Eigenvalues location as a function of speed within BFF model

This twofold behavior can be explained observing the root locus of two aircraft configurations as speed varies. Tail distance D is for both cases equal to 5m, while the bending stiffness parameter σ_s is equal to 0.6 in one case and to 0.12 in the other. In Fig. 5 the modes branches are identified (and labeled) according to their genesis of pure rigid-body or pure elastic modes. For the first aircraft configuration, depicted in Fig. 5(a), the eigenvalues of the system exhibit a pattern qualitatively similar to the one already shown in Fig. 2 for a

restrained wing model. In fact the flutter mechanism doesn't involve rigid-body coupling and it is the torsional mode which goes unstable (at V_f=146.7 $\frac{m}{s}$ and ω=75.3 $\frac{rad}{s}$).
However, when bending flexibility becomes more prominent (i.e. case with σ_s=0.12) two distinctive flutter mechanisms can be observed in Fig. 5(b). The first imaginary axis crossing takes place at a speed V_{f1}=150.3 $\frac{m}{s}$; this low frequency instability (ω_1=12.3$\frac{rad}{s}$) is a result of the interaction between short-period and bending modes (that is, the Body Freedom Flutter). The second crossing takes place at V_{f2}=162.8 $\frac{m}{s}$ at a higher frequency (ω_2=69.3$\frac{rad}{s}$) and is dominated by the bending-torsion instability already encountered.
In conclusion, the trend depicted in Fig. 4 is motivated by a change in the mode reaching earlier the flutter condition, which for the curves D=5,8m in the left side is the rigid-elastic coupled mode, while in the other cases is still the torsional mode.

V. Robust Analysis

Robust flutter analysis [5] deals with flutter instability predictions when the aeroelastic model is subject to uncertainties. Examples of the latter are low confidence in the values of parameters and coefficients of the matrices, or neglected dynamics in the nominal model. Once the problem is described within the LFT framework, μ analysis enables to predict for a given speed if the set of uncertainties is capable to lead to instability. As an introduction to this final section, a very brief description of these tools is provided (see [4] and references therein).

A. LFT and μ analysis

The *coefficient matrix* $\mathbf{M}$ is defined as a proper transfer matrix. $\mathcal{F}_u$, namely the upper LFT, is then the closed-loop transfer matrix from input $\mathbf{u}$ to output $\mathbf{y}$ when the nominal plant $\mathbf{M_{22}}$ is subject to a perturbation matrix $\mathbf{\Delta}$ (Fig. 6).

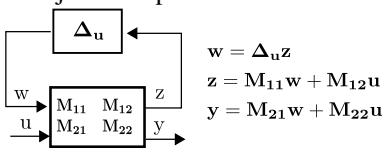

Fig. 6. Upper LFT

$\mathbf{M_{11}}$,$\mathbf{M_{12}}$ and $\mathbf{M_{21}}$ reflect a priori knowledge of how the perturbation affects the nominal map. Once all varying or uncertain parameters are *pulled out* of the nominal plant, the problem appears as a nominal system subject to an artificial feedback. The algebraic expression for $\mathcal{F}_u$ is given by:

$$\mathcal{F}_u(\mathbf{M}, \mathbf{\Delta_u}) = \mathbf{M_{22}} + \mathbf{M_{21}}\mathbf{\Delta_u}(\mathbf{I} - \mathbf{M_{11}}\mathbf{\Delta_u})^{-1}\mathbf{M_{12}} \quad (13)$$

This LFT is well posed if and only if the inverse of $(\mathbf{I} - \mathbf{M_{11}}\mathbf{\Delta_u})$ exists.

The structured singular value $\mu_\Delta(M)$ of a matrix $M \in C^{n\times n}$ with respect to the uncertain matrix Δ is:

$$\mu_\Delta(M) = \frac{1}{\min_\Delta(\bar{\sigma}(\Delta) : \det(I - M\Delta) = 0)} \quad (14)$$

where $\bar{\sigma}(\Delta)$ is the maximum singular value of Δ and $\mu_\Delta(M) = 0$ if there is no Δ satisfying the determinant condition. Note that this definition can be specialized to determine whether the LFT $\mathcal{F}_u(\mathbf{M}, \mathbf{\Delta})$ is well posed once the generic matrix M in the above definition is replaced by $\mathbf{M_{11}}$ and Δ belongs to the corresponding uncertainty set $\mathbf{\Delta}$. For ease of calculation and interpretation, this set is typically norm-bounded $\|\Delta\|_\infty < 1$ (without loss of generality by scaling of M). In this manner, if $\mu_\Delta(M) \leq 1$ then the result guarantees that the analyzed system is robustly stable (RS) to the considered uncertainty.

B. Results

Recalling last section, the matrix used by μ analysis to address the well-posedness is $\mathbf{M_{11}}$. This is the transfer function from the signal $\mathbf{w}$ to $\mathbf{z}$ associated to the LFT expression of the uncertain plant. Since the BFF problem is here formulated in the frequency-domain (11), once the uncertainties are introduced and the nominal dynamics is separated from the unknown terms, it is possible to build $\mathbf{M_{11}}$ from its definition (see [6] for a comprehensive description of the algorithm). This procedure implies a gridding of the frequency range under investigation: for each frequency value ω the terms involved in the definition of $\mathbf{M_{11}}$ are constant matrices and then the algorithm for the calculation of μ can be initialized.

The BFF robust stability test case is formed by using parametric uncertainties in D (nominal value corresponding to 6 m), EI (nominal value corresponding to σ_s=0.15) and three terms of the AIC matrix (the uncertain description is such that they range in the disc of the complex plane centered at the nominal value and having a radius equal to 3%). A small amount of aerodynamic uncertainty is included since it considerably enhances the numerical accuracy of μ_{LB}. The resulting upper LFT is defined by the nominal plant (11) and the relative uncertain block

$$\mathbf{\Delta} = \text{diag}(\delta_D I_7, \delta_{EI}, \delta_{A_{12}}, \delta_{A_{21}}, \delta_{A_{22}}) \quad (15)$$

where I is the identity matrix indicating the number of repeated uncertainties in the Δ-structure. The flutter speed V_f for the nominal plant is 162 $\frac{m}{s}$.

The goal is to show that μ analysis can be used to infer the conclusions discussed above with respect to BFF phenomena. This is done by assessing the role played by each uncertainty in the BFF RS calculation, i.e. a type of parametric sensitivity analysis performed in this case within the μ analysis framework. If a generic uncertain parameter C is considered, σ_C is used to define the uncertainty level and its relation with the nominal value C^0 is written as $C = C^0(1 + \sigma_C\delta_C)$.
In Fig. 7 the analysis at 150 $\frac{m}{s}$ with two different levels of uncertainty is shown. Since the upper and lower bounds are close in each case, only the former are plotted for clarity.
When the first uncertainty level set is considered (σ_{EI}=0.3 and σ_D=0.2), the instability detected by μ analysis is distinctly the BFF, as testified by the peak frequency ω_1 (slightly greater than 10$\frac{rad}{s}$). Moreover, μ_{LB} analysis provides an expression of the critical perturbation matrix $\mathbf{\Delta_{cr}}$, which shows that the instability is reached through a *reduction*

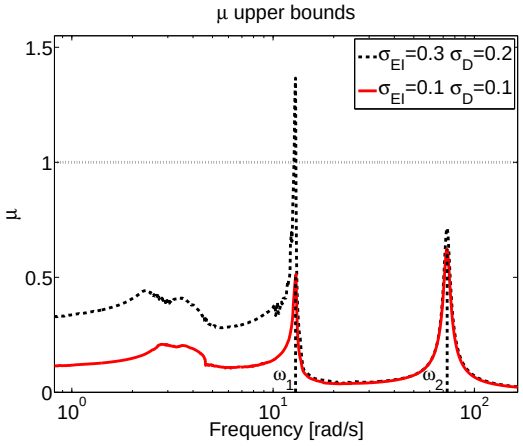

Fig. 7. Robust analysis at V=150$\frac{m}{s}$: μ_{UB} for two different sets of uncertainty level in stiffness σ_{EI} and tail distance σ_D

of both EI and D (negative values for δ_{EI} and δ_D), in accordance to Fig. 4. The other peak at ω_2 denotes the flutter mechanism due to the torsion-bending coupling, which is not critical for this plant, as testified by the μ value lower than 1. The examination of $\mathbf{\Delta_{cr}}$ at ω_2 reveals that a positive perturbation δ_{EI} is predicted. This agrees with this flutter mechanism, for which as previously commented instability is more pronounced as the bending stiffness is increased and thus bending and torsional frequencies become closer.

The analysis performed with the second (reduced) uncertainty level set (σ_{EI}=0.1 and σ_D=0.1) shows that this change barely influences the peak at ω_2, while the peak at ω_1 is highly affected. The behavior pointed out by μ analysis reflects the fact that for the BFF instability (low frequency peak) EI and D play a crucial role and thus a change in the uncertainty levels considerably affects the RS of the plant, while the torsional-bending instability (high frequency peak) is less dependent on them.

This analysis shows that once the plant described in (11) is recast in the robust analysis framework through LFT modeling, μ analysis enables both: (i) to quantitatively assess the effect of the different parameters on RS, and (ii) to infer the type of instability that is taking place. The above observations in fact provide a different perspective on the same features outlined in Section IV through Figs. 4-5 and the corresponding comments. However, when dealing with either more complex models or a greater number of variables, a parametric study as the one performed in Fig. 4 can become rapidly ineffective. The work presented in [13] is an example of sensitivity study of aeroservoelastic system affected by model uncertainties. Further investigations within the presented framework (not shown here due to space limitations), which include examination of other effects and additional uncertain parameters such as wing mass, confirms that μ analysis can cope with the additional complexity and still provide invaluable understanding.

VI. Conclusion

This work investigates the Body Freedom Flutter (BFF) phenomena, affecting mainly flexible aircraft configurations with adverse geometric properties. First, the capability of the typical section aeroelastic framework in studying the flutter of a cantilever wing (restrained flutter) was demonstrated with the Goland wing benchmark. Following the presentation of a simple model capturing the basic features of BFF, a conventional air vehicle configuration (wing/fuselage/tail) was studied with a standard flutter algorithm (p-k method) focusing on the effect of two key parameters, wing bending stiffness and horizontal tail distance from the nose. Among other things, this parametric study showed that there is a range of wing bending flexibility where the rigid elastic coupling is not relevant and the instability predicted by the BFF model closely resembles the one obtained with the restrained wing assumption. As the flexibility increases, the tail distance turns to be meaningful for the destabilizing mechanism and the rigid-bending mode becomes the one reaching earlier the flutter condition.

Finally, robust analysis is performed to study the plant when it is affected by uncertain parameters. It is shown that the same observations obtained with the previous parametric analysis can be inferred employing μ technique. Indeed, μ analysis is able to quantitatively assess stability degradation due to uncertainties in the models, as shown also in other works. Compared to these, the present contribution focuses more on: the LFT-oriented approach adopted to model the plant, the detection of two distinct mechanisms leading to flutter and the attempt to reconcile numerical analyses (both nominal and robust) with physical effects, gaining an insight on the type of instability affecting the system.

References

[1] E. Burnett, C. Atkinson, J. Beranek, B. Sibbitt, B. Holm-Hansen, and L. Nicolai, "NDOF Simulation Model for Flight Control Development with Flight Test Correlation." AIAA Modeling and Simulation Technologies Conference, Guidance, Navigation, and Control, 2-5 August 2010.

[2] D. Schmidt, "MATLAB-Based Flight-Dynamics and Flutter Modeling of a Flexible Flying-Wing Research Drone," *Journal of Aircraft*, 2015.

[3] C. Pettit, "Uncertainty Quantification in Aeroelasticity: Recent Results and Research Challenges," *Journal of Aircraft*, no. 5, 2004.

[4] G. Balas, J. Doyle, K. Glover, A. Packard, and R. Smith, *μ Analysis and Synthesis Toolbox*, 1998.

[5] R. Lind and M. Brenner, *Robust Aeroservoelastic Stability Analysis*, ser. Advances in Industrial Control. Springer London, 2012.

[6] D. Borglund, "The μ-k method for robust flutter solutions," *Journal of Aircraft*, vol. 41, no. 5, pp. 1209–1216, 2004.

[7] R. L. Bisplinghoff and H. Ashley, *Principles of Aeroelasticity*. New York: Wiley, 1962.

[8] M. Goland, "The flutter of a uniform cantilever wing," *Journal of Applied Mechanics*, vol. 12, no. 4, 1945.

[9] J. Banerjee, "Explicit Frequency Equation and Mode Shapes of a Cantilever Beam Coupled In Bending And Torsion," *Journal of Sound and Vibration*, 1999.

[10] D. Schmidt, *Modern Flight Dynamics*. McGraw-Hill, 2012.

[11] M. J. Patil, D. Hodges, and C. Cesnik, "Nonlinear Aeroelasticity and Flight Dynamics of High-Altitude Long-Endurance Aircraft," *Journal of Aircraft*, vol. 38, no. 1, pp. 88–94, 2001.

[12] M. Love, P. Scott Zink, and P. Wieselmann, "Body freedom flutter of high aspect ratio flyingwings." 46th AIAA/ASME/ASCE/AHS/ASC Structures, Structural Dynamics & Materials Conference, 18-21 April 2005.

[13] A. Kotikalpudi, H. Pfifer, and P. Seiler, "Sensitivity of Robust Flutter Boundary to Model Uncertainties in Aeroservoelastic Systems," in *AIAA Science and Technology Forum and Exposition*, 2016, pp. Paper No. AIAA–2016–1752.